Crystallization of Poly(L-lactic acid) on Water

Surfaces via Controlled Solvent Evaporation and

Langmuir Blodgett Films

Qian Qian, Carl T. Furner, Christopher Y. Li*

Department of Materials Science and Engineering, Drexel University, Philadelphia, Pennsylvania

19104, United States

KEYWORDS: Polymer crystallization, polymer single crystals, evaporative crystallization, water surface, Langmuir-

Blodgett film

Abstract. Solvent evaporation is one of the most fundamental processes in soft matter. Structures

formed via solvent evaporation are often complex yet tunable via the competition between solute

diffusion and solvent evaporation time scales. This work concerns the polymer evaporative

crystallization on water surface (ECWS). The dynamic and two-dimensional nature of the water

surface offers a unique way to control the crystallization pathway of polymeric materials. Using

1

poly(L-lactic acid) (PLLA) as the model polymer, we demonstrate that both one-dimensional (1D) crystalline filaments and two-dimensional (2D) lamellae are formed via ECWS, in stark contrast to the 2D Langmuir-Blodgett monolayer systems as well as polymer solution crystallization. Results show that this filament-lamella biphasic structure is tunable via chemical structures such as molecular weight and processing conditions such as temperature and evaporation rate.

Introduction

Evaporation-induced self-assembly of soft matter has been extensively investigated.¹⁻⁹ For example, nanoparticles are directed to organize into desired structures by controlling solvent evaporation time and particle flow during evaporation. Phase transformation during solvent evaporation is a rich field to study and is tunable by the Peclet number Pe (Pe = τ_D/τ_{EV} , where τ_D and τ_{EV} are the solute diffusion and solvent evaporation time scales, respectively.¹⁰⁻¹² This

phenomenon is fundamental in various fields, including materials science and chemistry, influencing processes like crystallization, precipitation, and film formation. ¹³⁻¹⁵ In particular, evaporative crystallization has been explored and used in industry for decades. In the field of polymers, evaporative crystallization was used to monitor polymer spherulites growth and the crystallization process in thin films and sessile droplets. ¹⁶⁻²²

One of the intriguing research directions in polymer crystallization deals with controlling polymer crystallization pathways via external means, such as confinement or introducing precise defects to the polymer chain. ^{1-3, 9, 23} In particular, curved water/oil interfaces in nanoemulsion guide polymer crystal growth to form hollow crystalline particles known as crystalsomes.²⁴⁻³² Polymer crystallization on water surfaces has been extensively investigated using the Langmuir-Blodgett (LB) approach. In this case, a true 2D polymer film is formed on the water surface, and the polymer crystallizes upon compression of the LB film. Both flat-on and edge-on crystals have been observed in polycaprolactone (PCL)³³⁻³⁷ and poly (L-lactic acid) (PLLA),³⁸⁻⁴³ respectively. Detailed morphological evolution in PLLA LB films has been systematically studied.³⁸⁻⁴³ ^{42, 43} Fractal crystal morphology was seen in giant surfactant LB films. 44, 45 Most recently, evaporative crystallization on water surfaces (ECWS) was reported as an alternative method to the established LB approach to study polymer crystallization on water surfaces. 46, 47 Compared to the molecular monolayer of LB film, ECWS deals with a quasi-2D system, where a sub-millimeter-thick organic phase (polymer solution) is formed atop the water. Evaporation of the solvent leads to a shift on the phase diagram by increasing concentration and eventually leads to crystallization at and/or near the water surface. This phase front moves orthogonally to the water surface, contrasting the lateral pressing method used in LB. One can also change polymer solution concentration, solvent type, temperature, and evaporation rate to control the crystallization pathways.

Previously, we showed that when a telechelic PCL with terminal carboxylic acid groups is used in ECWS, the two hydrophilic chain ends are pinned at the organic/water interface, which alters the chain conformation prior to crystallization.⁴⁶ The pinning of the chain ends affects the crystallization pathway and changes the fold number of the final 2D lamellae. The resultant 2D single crystal sheet was proven Janus as all the carboxylic acids groups were located on one side of the crystals. When PLLA is used in ECWS, it is found that both 1D and 2D crystals are formed, while 2D lamellae are found in solution crystallization, and 1D fibrillar crystals are observed in the LB systems.⁴⁷ The observed 1D-2D biphasic morphology suggests the complexity of the ECWS process. To better understand and tune the ECWS process, in this work we investigated the PLLA ECWS using ultra-fast evaporation (<1 min). Results are compared with the slow evaporation ECWS and the crystallization process in LB systems. Our results show that 1D PLLA crystals are exclusively formed in the fast evaporation ECWS of PLLA, consistent with the crystallization behavior in LB. The absence of 2D crystals in the fast evaporation ECWS confirms that the 2D crystals formed in slow ECWS are formed in the residual solution phase, where chains are less confined. Post-crystallization annealing shows that 2D lamellae are the thermodynamically more stable phase. Temperature and molecular weight also play a critical role in PLLA structural formation on water.

Experimental Section

Materials. PLLA and poly(L, D-lactic acid) (PLDLA) samples (PLLA number average molar masses M_n of 2 kDa and 10 kDa with disparities D of 1.25, and 1.10; PLDLA $M_n = 10$ kDa, D = 1.19) were purchased from Polymer Source, and high molecular weight PLLA samples ($M_n = 100$ kDa, D = 1.30) were purchased from NatureWorks. Toluene (ACS, 99.5%) was purchased from

Aldrich and used after distillation. DI water was purified by a Milli-Q system and used as the subphase for ECWS. Micro Cover Glasses (VWR) were used as the substrate to collect samples on the water surface for atomic force microscopy (AFM) imaging. The glass slides were treated in piranha solution (3:1 v/v, 98% H₂SO₄/35% H₂O₂) at room temperature for 8 h and kept in DI water; glass substrates were dried with nitrogen gas before use.

Sample preparation. PLLA/toluene solution was prepared by dissolving PLLA in toluene at 80 °C and cooled to room temperature for 15 min before ECWS. Different concentrations of PLLA/toluene solution (0.01, 0.03, 0.05, 0.1, and 1 wt.%) were prepared at the same condition. PLLA/toluene solution was added dropwise on the water surface in a 100 mL beaker with 80mL DI water. The beaker was then placed in air for ECWS, samples were collected at different time points using a Blodgett-Schaefer-type method with the cleaned glass slides mentioned above. To measure surface tension in ECWS, 1000 mL beakers were used to produce a stable reading.

For polymer crystallization using LB, the polymer LB film was prepared with a standard Langmuir trough (KSV 5000, Biolin Scientific, Ltd.). The LB trough and barriers were cleaned and the trough was filled with ultrapure 18.2 M Ω water (Millipore, Milli-Q Gradient A-10) to make the water surface at the same level as the edges of the trough. The cleaning procedure was repeated multiple times until the surface pressure at the minimum trough area was less than 0.2 mN/m during the compression and expansion process. Surface pressure was recorded by the Wilhelmy plate technique. A platinum plate (39.24 mm) was used as the Wilhelmy plate and connected to a balance for the reading of surface pressure. In a typical procedure, 30uL of 0.6wt% PLLA/toluene solution was added on top water surface in LB trough to make the initial average area occupied by the monomer of PLLA equal to 0.45 nm²/ru. After adding the solution, the LB trough stood still for at least 20 min to allow for the evaporation of solution and spreading of

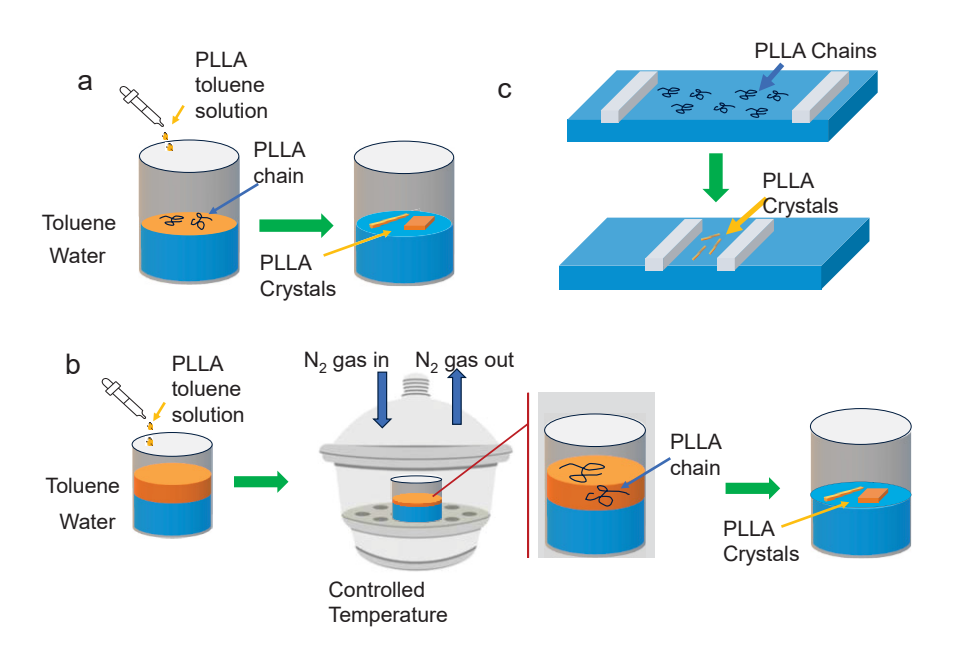
polymer on surface, then the barriers started to compress with a rate of 0.05mm/s, and the Π -A isotherm was recorded.

AFM samples were prepared by using a pre-cleaned cover glass to collect the polymer film following the Blodgett-Schaefer-type method when the surface pressure reached the set values (1, 3, 7, 9 and, 12 mN/m). For each batch of the sample, the trough was cleaned and prepared using the same amount of DI water and solution.

Characterization. The morphology analysis was performed by AFM using a Bruker Multimode 8 instrument with the PeakForce Tapping (PFT) mode in air at room temperature. The radius of curvature of the silicon nitride cantilever (SCANASYST-AIR) used was ~2 nm. The prepared polymer samples on glass slides were dried in vacuum for at least 24 h before imaging. Images were acquired at a scanning rate of ~ 1.0 Hz per line with the resolution of 256 × 256 pixels and analyzed using NanoScope Analysis v1.8. For each crystallization condition, samples were collected at three locations on the water surface and scanned with AFM. Transmission electron microscopy (TEM) experiments were performed using a JEOL JEM-2100 LaB6 TEM at a voltage of 120kV. TEM samples were prepared by collecting polymer films on the water surface using carbon-coated copper grids following the Langmuir-Blodgett deposition method. The samples were then dried in vacuum for at least 72 h before imaging. TEM images and selected area electron diffraction (SAED) patterns were analyzed with Gatan Microscopy Suite v3.5 and ImageJ.

Results and Discussion

Scheme 1 depicts the experimental procedures of the fast and slow ECWS as well as crystallization in LB films for comparison. In the fast ECWS, an aliquot of PLLA solution in toluene (~10- 30 μL, 0.03 wt. %) is added onto the water surface in a 100 mL beaker housed in an ambient environment. Because of the small amount of solvent, it takes approximately 6 sec for the solvent to evaporate (Scheme 1a, See later surface pressure results). In the slow ECWS experiment, one gram of toluene is added to create a 100s-μm-thick organic phase before the polymer solution is introduced, and the evaporation time is a few h (Scheme 1b). Crystallization of an LB film is shown in Scheme 1c, where the organic solvent is removed before compressing the LB barriers and the lateral compression of the LB barriers induces the crystallization process. Table 1 summarizes the typical characteristics of the three methods.



Scheme 1. Schematics of fast (a) and slow (b) evaporative crystallization on water surface used in this work. (c) Polymer crystallization on the water surface in LB.

Table 1. Characteristics of fast, slow ECWS and polymer crystallization in LB films.

	Organic Phase Amount	Organic Phase Thickness	Total Evaporation Time	Lateral Compression	Morphology	Crystal thickness
F-ECWS ^a	< 100 μL	<60 μm	~ mins	No	1D	~0.8-12 nm
S-ECWS ^b	~1 mL	~600-700 μm	3-10 h	No	1D, 2D	~0.8-20 nm
C-LB ^c	-	-	-	Yes	1D	$\sim 0.86 \; nm$

a. F-ECWS: fast evaporative crystallization on water surface

Upon evaporation of toluene in the fast ECWS, the film was picked up using a Langmuir-Shaefer method onto a pre-cleaned cover glass for AFM study. **Figure 1a-c** depicts, at different magnifications, samples collected 1 min after adding the PLLA solution onto the water surface. The entire surface is covered by thin filaments. These filaments appear to be bimodal in terms of their thickness. There are a few long ~ 3 nm thick filaments, and the majority are much thinner (1-2 nm) ones. These filaments are locally aligned with a nematic-like order, and the thinner filaments are shorter. Remarkably, they also tend to link together along the filament axis, merging to form a longer 1D fiber, which is consistent with the previously proposed particle-mediated growth mechanism. The 1D filament morphology is retained in the samples picked up 15 min after the deposition of the PLLA solution (**Figure 1d-f**). Furthermore, their thickness becomes much

b. S-ECWS: slow evaporative crystallization on water surface

c. C-LB: Crystallization of LB films on water surface

more uniform, approximately 3 nm. This observation suggests that **Figure 1a-c** represents the intermediate state of the 1D filament growth.

A control experiment was conducted to identify the role of crystallization in the 1D filament formation process. PLDLA is noncrystalline since it is racemic, formed by copolymerization of L- and D- lactide monomers. PLDLA was then utilized following the same fast ECWS process. As shown in **Figure 1j**, only isotropic clusters were formed 15 min after the deposition. The average cluster size is ~ 20 nm, and the average height is ~ 2.5 nm. In **Figure 1g**, similar round clusters appear at t = 1 h for 10 kDa PLLA. These clusters then serve as the nuclei for crystallization of PLLA to form 1D filaments. These clusters, however, appear to be the terminal morphology when the polymer is noncrystallizable as in PLDLA as demonstrated in **Figure 1j**. The results suggest that the formation of laterally isotropic clusters in the first step is universal for crystalline and noncrystalline PLLA, and therefore, crystallization is the driving force to form 1D filament.

To better understand the fast ECWS process, the surface pressure was monitored using a Wilhelmy plate method, and the results are shown in **Figure 2**. Upon adding 10 μ L of PLLA solution, the surface pressure immediately increases and stabilizes after ~ 6 sec. The surface pressure is defined as the drop in surface tension of water when a polymer solution is introduced, $\Pi = \gamma_{w0} - \gamma_{w1}$ (where Π , γ_{w0} , γ_{w1} denote surface pressure, water surface tension before and after adding the PLLA solution, respectively). With the PLLA concentration changing from 0.01 to 0.05 wt.%, the surface pressure increase ($\Delta\Pi$) also varies from ~ 13.5 to 16.3 mN/M². $\Delta\Pi$ in the fast ECWS is greater than those observed in the slow ECWS case (dotted line in the figure). (Note that to measure the interfacial tension, the system was scaled up by adding 62.2g of toluene atop 800mL

of DI water to create a \sim 1.2 cm thick toluene layer). $\Delta\Pi$ in the slow ECWS is attributed to the PLLA molecules adsorbed onto the interface, while in the fast ECWS case, the surface pressure of water/air interface is measured, and both toluene and PLLA molecules contribute to $\Delta\Pi$. It is also interesting to note that in the fast ECWS case, the surface pressure quickly drops again after \sim 200 sec and approaches a steady region after \sim 15 min. In the slow ECWS case, the surface pressure does not show a noticeable change within this time scale. The surface pressure drop in the fast ECWS can be attributed to toluene evaporation on the water surface. Due to the much larger amount of toluene used , Π in the slow ECWS measure the toluene/water interface, and no obvious drop was observed. This surface tension drop offers a good marker for understanding the 1D crystal formation process.

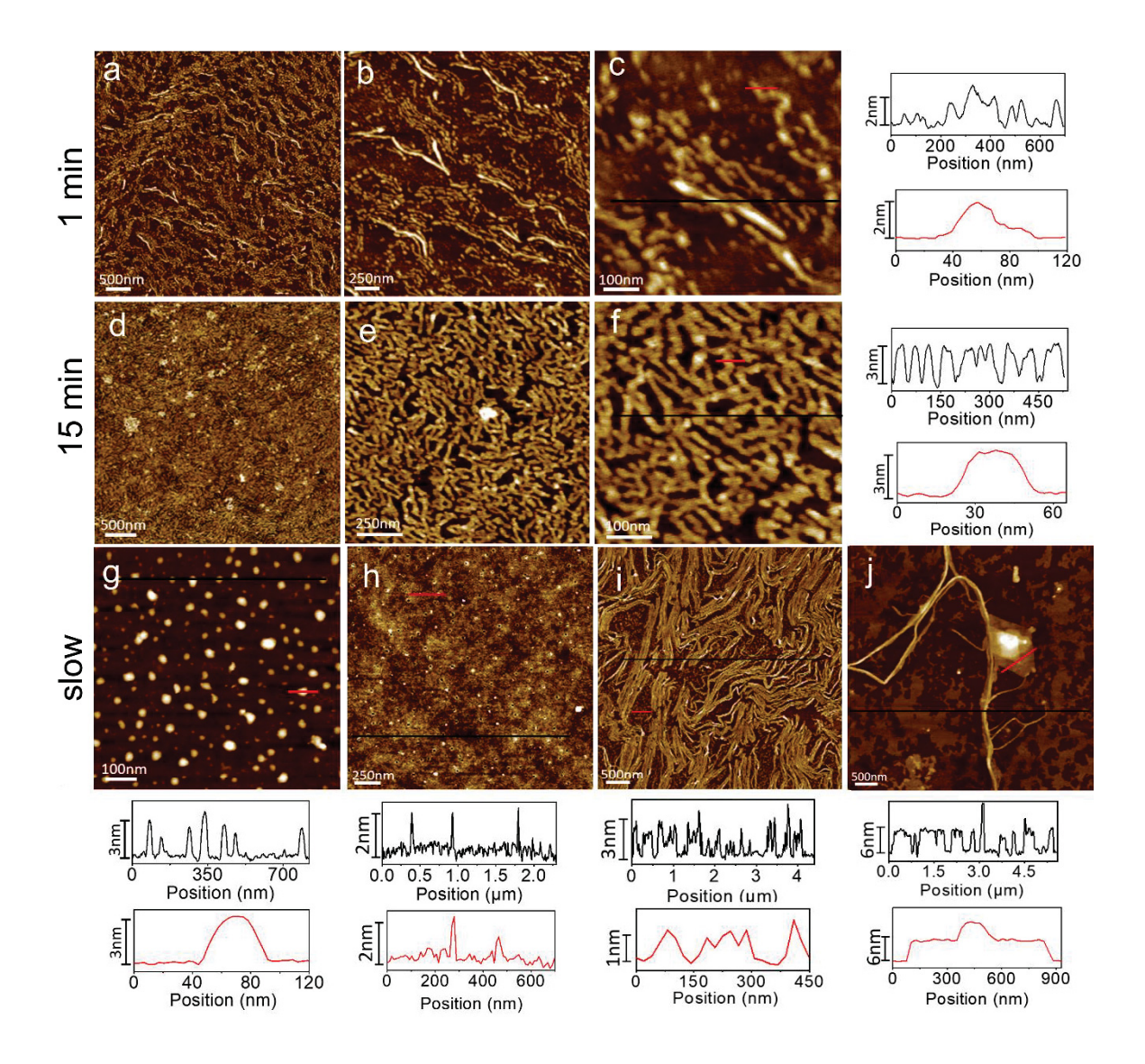


Figure 1. AFM images of 10 kDa PLLA crystals formed by fast (a-f) and slow (g-i) ECWS at 21 °C. (a-c) are height images, at different magnifications, of the samples collected 1 min after adding 10 μL of 0.03 wt. % PLLA/toluene solution to the water surface. (d-f) are height images, at different magnifications, of the samples collected 15 min after adding 10 μL of 0.03 wt. % PLLA/toluene solution to the water surface. The height profiles on the right panels correspond to (c) and (f), respectively. (g-i) AFM height images with corresponding height profiles of 10 kDa PLLA crystals formed by slow ECWS at 21 °C. The samples for the images were collected 1 h (g), 3 h (h), and 7 h (i) after adding PLLA solution to preformed toluene/water bilayer. (j) AFM images and the corresponding height profiles of PLDLA clusters formed by fast ECWS at 21 °C. (images g-i were adapted from Ref. 47).

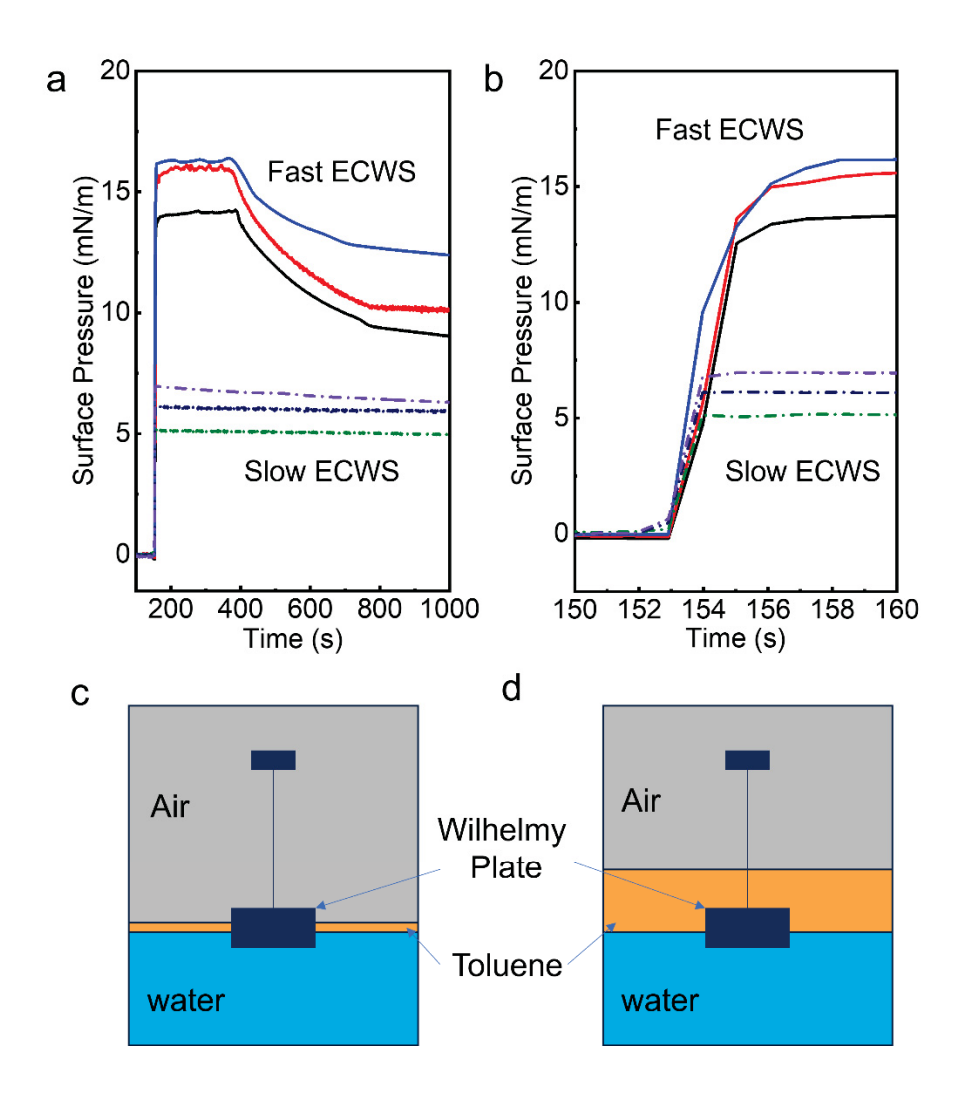


Figure 2. Surface/interface pressure upon introducing PLLA solutions measured using the Wilhelmy plate method. Solid and dotted lines are from fast and slow ECWS, respectively. In each case, from bottom to top, 10 μL of 10 kDa PLLA solutions with a concentration of 0.01, 0.03 and 0.05 wt.% were added to the water surface (fast ECWS) or a pre-formed toluene/water bilayer (slow ECWS) at 21 °C. (b) is an enlarged view of (a), highlighting the rapid surface/interface pressure changed upon adding the PLLA solution. Red arrows indicate the time at which PLLA solution was added. (c-d) are experimental set-up to measure the interfacial tension in fast ECWS (c) and slow ECWS (d).

Taking together the surface pressure and morphology results, we can conclude that in the fast ECWS process, 1D crystals form quickly after the PLLA solution is added atop the water surface (1 min, red arrow in **Figure 2**), the crystals continuously grow as the toluene phase

evaporates, and finally evolve into 1D crystals with a thickness of ~ 3 nm (3-4 layer of PLLA molecules). The crystal evolution in the slow ECWS was previously reported, ⁴⁷ and the typical morphologies are reproduced in Figure 1g-i, representing 10 kDa PLLA crystals formed in slow ECWS 1, 3, and 7 h after adding the polymer solution to the system. Comparing the slow and fast ECWS, the major differences are twofold. (1) The final morphology in slow ECWS is a biphasic structure with both 1D filaments and 2D lamellae (see Figure 1i). (2) The time scale of the structure formation is quite different. While the terminal 1D filament morphology is observed within 15 min in the fast ECWS, the 1D filaments are formed after 3 h, and the 2D lamellae are formed towards the end of the evaporation (6-7 h) in the slow ECWS process. We attributed the formation of 2D lamellae of 10 kDa PLLA to the potential crystallization in the solution phase, where interfacial confinement is weak.⁴⁷ The lack of 2D lamellae in the fast ECWS further confirms this hypothesis: due to the fast evaporation kinetics and the small amount of toluene used, solution crystallization was completely bypassed, and all crystals are formed under the strong confinement of the water surface, leading to the uniform 1D filament morphology. The results also confirm the nucleation-merging process of the 1D filament.

While **Figure 1** shows the formation of 1D filament in fast ECWS, the nucleation stage (cluster formation) is not as clear as the slow ECWS case (**Figure 1a-c** vs. **Figure 1g**). This could be due to the local high concentration of PLLA molecules when adding the PLLA solution directly to the water surface. To confirm this hypothesis and mitigate the potential local high PLLA concentration, we utilized 100 μ L of 0.003 wt.% PLLA solution for fast ECWS. The total amount of PLLA molecules was kept the same while the concentration was decreased 10 times by dilution. **Figure 3a-h** depicts the AFM images of samples collected at 1, 15 min, and 24, 30, 36, 42, and 48 h, respectively. Clusters with a height of ~ 2 nm can be seen in the 1 min sample, mimicking the

early stage of the slow ECWS (**Figure 1h**). This observation confirms that **Figure 1a-c** represents a more advanced stage of **Figure 3a**, which is likely due to the higher local polymer concentration in **Figure 1** fast ECWS. The filament morphology is maintained up to 24 h (**Figure 3b-c**). At 30 h, 2D lamellae appear and progressively become the dominant morphology for samples collected after 36 h (**Figure S1**). Single layer lamellae have a thickness of ~ 6 nm, while much thicker multilayers can be seen for samples annealed for 48 h (**Figure 3g and S2**). Note that the formation of 2D crystals after long time of annealing at 21 °C on water surface can also be observed in samples from 10 μL 0.03 wt.% fast ECWS (**Figure 3h**). Lozenge shaped overgrowth with a screw dislocation can be seen for ribbon-shaped crystals, suggesting significant chain rearrangement during the annealing process.

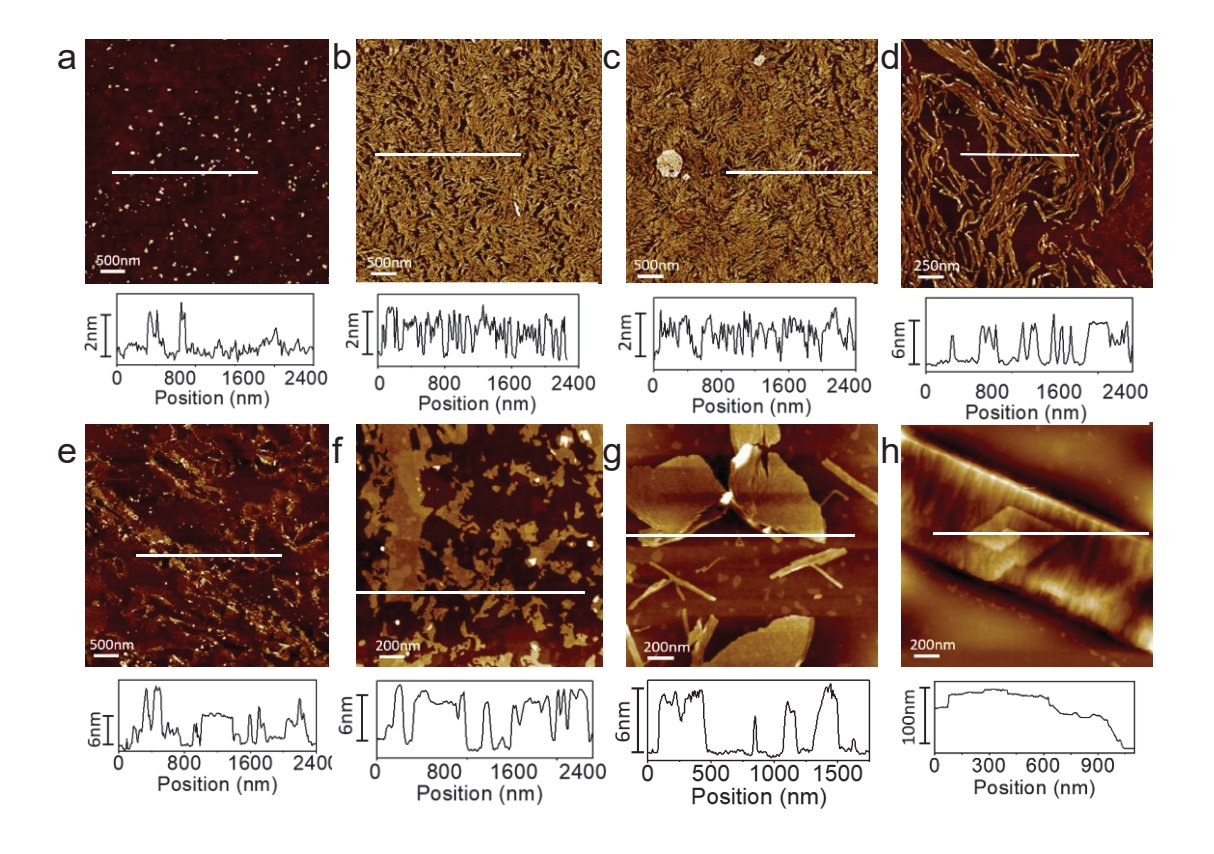


Figure 3. AFM images of 10 kDa PLLA crystals formed by fast ECWS at 21 °C by adding 100 μ L of 0.003 wt. % PLLA/toluene solution to the water surface. (a-g) were collected 1 min (a), 15 min (b), 24 h (c) 30 h (d) 36 h (e), 42 h (f), and 48 h (g) after adding the polymer solution. (h)

represent samples after extensive annealing (48 h) of the polymer crystals on the water surface using $10~\mu L$ of 0.03 wt. % PLLA/toluene solution.

Transmission electron microscopy (TEM) experiments were conducted to determine the chain orientation in these crystals. The filament morphology can be clearly seen under TEM. The SAED pattern shows a pair of (110) diffraction spots corresponding to the long axis of the filament, indicating that the polymer chains are orthogonal to the fibrillar direction, which is perpendicular to the (110) plane. This observation is consistent with the slow ECWS results. However, the 2D crystals formed after extensive annealing on the water surface produce a [00/] zone diffraction pattern based on the α phase PLLA unit cell (orthorhombic unit cell with a = 1.0683 nm, b = 0.6170 nm and c (chain axis) = 2.8860 nm, 53 as shown in **Figure 4c-d**. The above AFM and TEM results clearly suggest that on the water surface, 2D flat-on crystals are thermodynamically more stable, and the 1D filaments are formed due to the confinement of the water surface, which forces the PLLA chains to lie down on the water surface prior to crystallization. This effectively changes the crystallization pathway and leads to 1D crystals. The 1D-2D transition involves a chain orientation change and might be facilitated by the trace amount of free polymer chains on the water surface. The PLLA chains appear to have sufficient mobility at 21 °C on the water surface, and rearrange their orientation upon extensive (48h) annealing, forming 2D flat-on crystals.

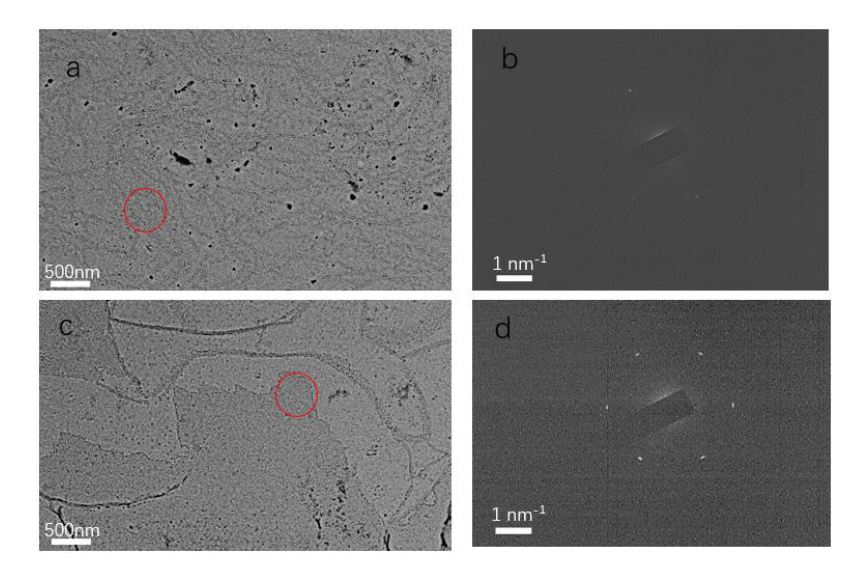


Figure 4. TEM images of the 10 kDa PLLA filaments collected 15 min after adding polymer solution (a) and its corresponding SAED pattern (b). (c) the 2D lamellar morphology for sample collected 48 h after adding the polymer solution. (d) SAED pattern of (c).

A few research groups have investigated classical PLLA crystallization on the water surface using the LB technique (C-LB).³⁸⁻⁴³ As listed in **Table 1**, there are similarities and differences between C-LB and ECWS. Specifically, in C-LB, the organic solvent (toluene in this case) is removed before the LB process, while the solvent plays a crucial role in determining the crystallization pathway in ECWS. Therefore, C-LB deals with a polymer monolayer while ECWS is a quasi-2D system, which allows for more complex polymer structural and morphological evolution. The crystallization process in C-LB is triggered by laterally reducing the surface area of the polymer monolayer. However, ECWS relies on the increased polymer concentration in the solution and at the liquid/liquid interface upon solvent evaporation. Note that ECWS can be conducted using an LB-trough when the compressing process is not applied.

To quantitatively compare C-LB (compression induced crystallization) and the ECWS (evaporation induced crystallization) processes, 10 kDa PLLA solution was added to an LB trough,

and a monolayer of PLLA in a 2D gas state was formed. An LB isotherm was obtained at 21 °C by laterally compressing the film as shown in **Figure 5**. The isotherm is consistent with previously reported results.³⁸⁻⁴³ The surface pressure Π gradually increases as the area per PLLA repeating unit increases. A plateau was obtained in the range of 0.13-0.17 nm²/ru, corresponding to a surface pressure of ~ 8.9 mN/m. These observations are consistent with the literature reports.³⁸⁻⁴³ Four samples were collected onto pre-cleaned glass slides using a Blodgett-Schaefer-type method, at the surface pressure of 1, 3, 7, and 9 mN/m, for AFM imaging. As shown in Figure 5b-e, at 1 mN/m, no obvious polymers were collected. Round particulate objects with a lateral dimension of 50 nm and thickness of 1nm can be seen at 3 mN/m. The round objects became anisotropic with an aspect ratio of 0.35 (~21 nm and 60 nm in width and length, respectively) at 7 mN/m. And aligned 1D filaments are seen at 9 mN/m. In the fast ECWS experiment, we used the initial polymer concentration/quantity to mimic the LB process as shown in Figure 5f-i. The total amount of polymer used was determined based on the targeted polymer surface area per repeating unit, and 10 µL of 0.01, 0.03, 0.05, and 0.1 wt. % of PLLA toluene solutions were utilized for ECWS. The 0.01 wt.% ECWS sample shows particles with a lateral size of 50nm and a height of ~ 1.5 nm. Uniform 1D filaments are seen for 0.03 and 0.05 wt. % samples, and these 1D filaments are ~ 3 nm in height. Complex, multilayered films are seen for 0.1 wt.% samples, and there are seemingly both 1D and 2D crystals. The multi-layered and 2D lamellae are more obvious and abundant in the 1 wt.% ECWS samples, shown in Figure 5g, h.

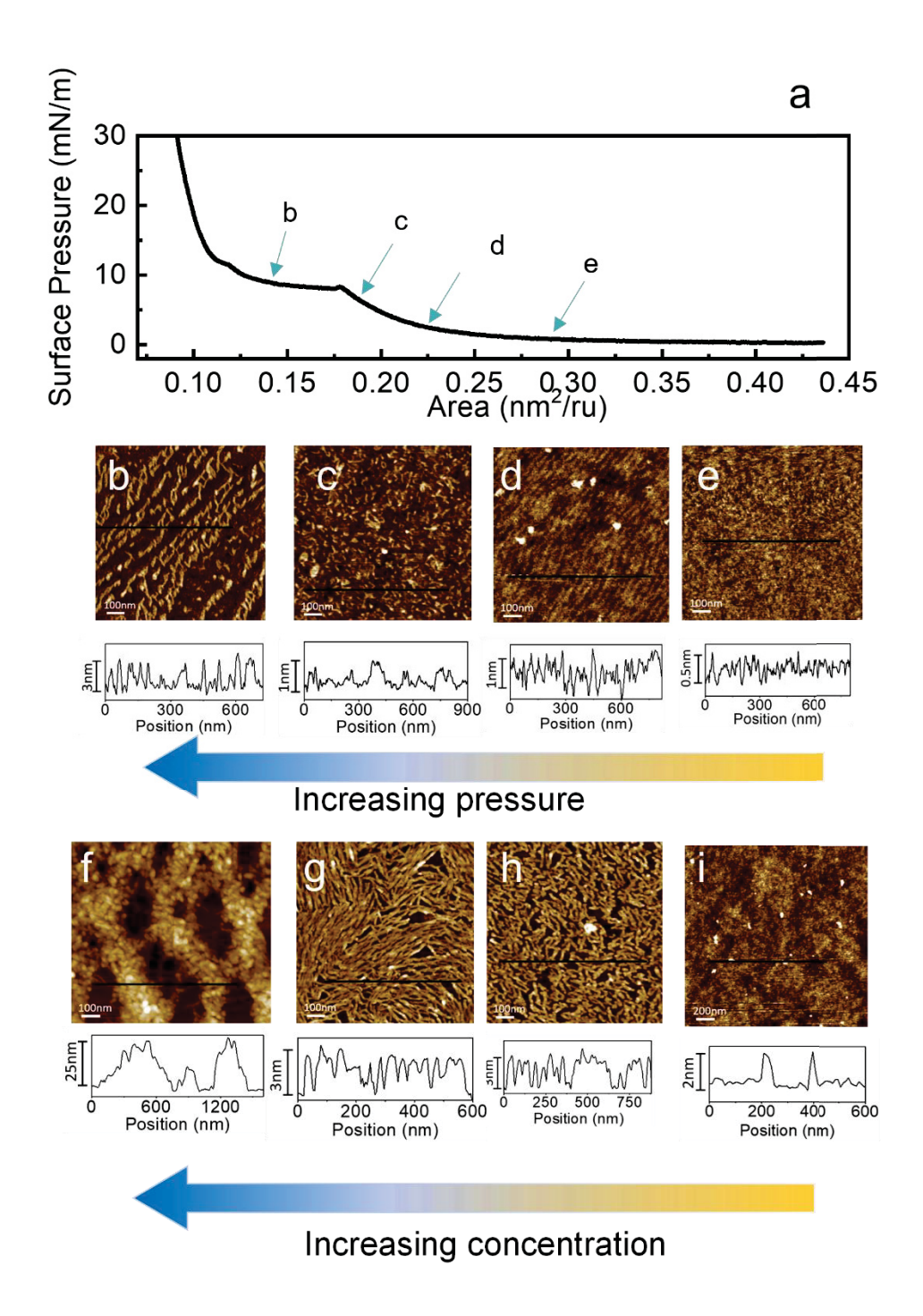


Figure 5. AFM images of 10 kDa PLLA crystals formed by fast ECWS in beaker and crystallization on LB at 21 °C (a) was the π –A isotherm of the monolayer with the compression rate of 0.05 mm/s. Arrows corresponding the AFM images b-e. (b-e) were AFM height images of the LB monolayer deposited on glass slide with the LS type method at the π of (b) 9mN/m, (c) 7mN/m, (d)3mN/m and (e) 1mN/m. (f-i) were AFM height images of the thin layer formed by fast evaporation ECWS with the concentration of (f) 0.1wt.%, (g) 0.05wt.%, (h) 0.03wt.%, and (i) 0.01wt.%.

Morphological comparison between the crystals formed by C-LB and ECWS demonstrates that the structural evolution of these two processes is similar, despite the intrinsic differences of these two methods highlighted in Table 1. In both cases, nucleation and growth of 1D crystalline filaments are observed at similar areas per repeating unit, suggesting that the ECWS can be used as an alternative method to C-LB for investigating crystallization on water surface. One major difference between the C-LB and the fast ECWS is that at a relatively high concentration such as 0.1 or 1 wt. %, 2D lamellae, which are absent in the C-LB, are formed. 2D lamellae are also seen in slow ECWS at the very end of the evaporation process. They are attributed to the crystallization in the organic phase or from polymers with less confinement/more facile desorption from the water surface. To this end, 10 µL, 0.03 wt. % of 2 kDa and 100 kDa PLLA were also used for fast ECWS, and the results are shown in Figure 6. The images in Figure 6a-c reveal that, for 2 kDa PLLA, the majority of crystals are 2D lamellae; some are lozenges, and some are irregular. A small fraction of the samples shows 1D filament morphology. In the case of 100 kDa PLLA, the majority of crystals are 1D filaments. Interestingly, the sample collected at 1 min clearly shows particles chaining in one direction, leading to 1D filament morphology. For samples collected at 15 min and 24 h, relatively smooth 1D filaments are seen. This observation is consistent with the slow ECWS results that a biphasic morphology consisting of 1D filaments and 2D lamellae are formed for 10 kDa and 100 kDa sample crystallization at 21 °C. The dominance of 2D crystals formed in 2 kDa samples is attributed to the easier collective desorption of ester groups from the water surface due to shorter polymer chains (hence fewer ester groups than 10 kDa and 100 kDa PLLA). Therefore, desorption of the ester groups generates upright chain conformation, which leads to 2D flat-on lamellae crystals, as shown in Figure 6d,h.

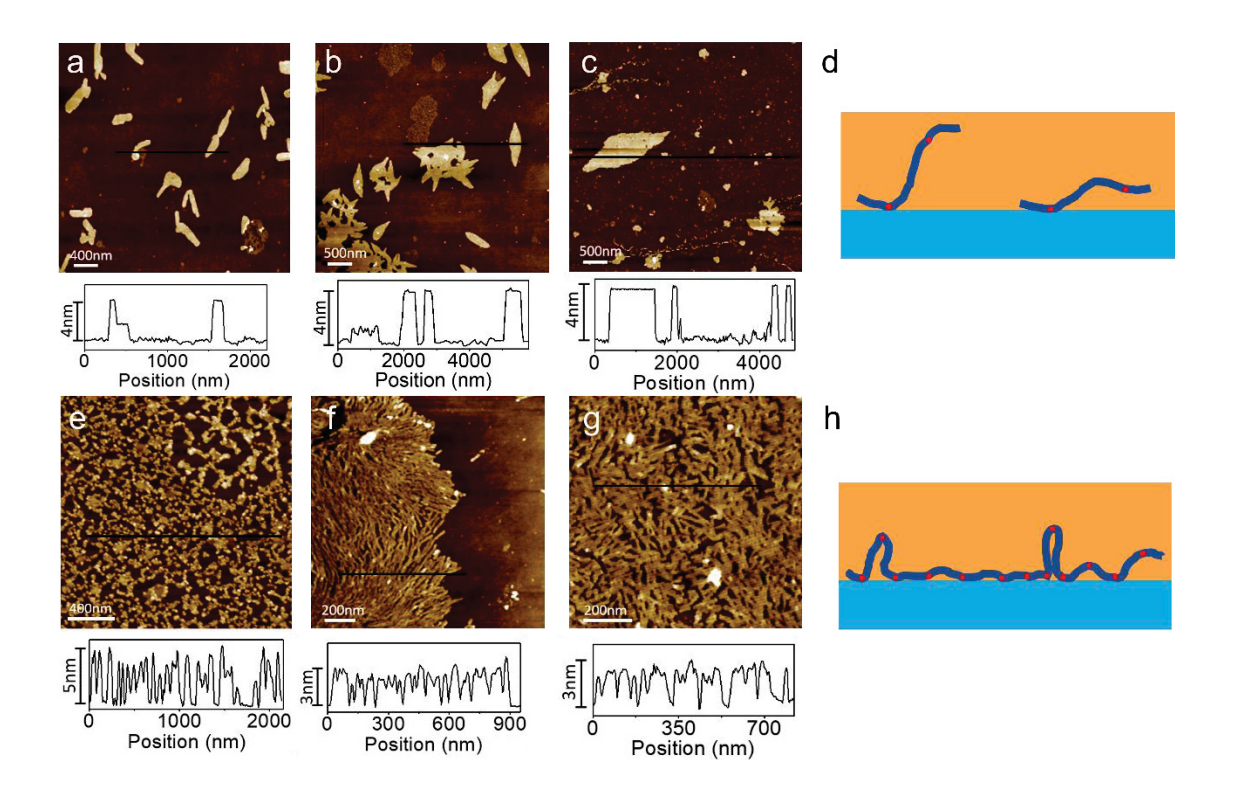


Figure 6. Molecular weight effect in fast ECWS. AFM images of polymer crystals formed using 10 μL 0.03% PLLA toluene solutions where PLLA MW is 2 kDa (a-c) and 100 kDa (e-g). The samples were collected at different time points, *i.e.* 1 min (a, e), 15 min (b, f), and 24 h (c, g), after adding the PLLA solution. (d, h) schematics of polymer chains confined on water surface for low MW (d) and high MW (h) PLLA.

One noticeable difference between the fast and slow ECWS is that for 10 kDa PLLA, fast ECWS led to 1D filaments while slow ECWS produced 1D filaments in the early stage and a biphasic morphology consisting of both 1D and 2D crystals in the late stage of the growth. This can be explained by the increasing polymer solution concentration in the late stage of slow ECWS. Once the concentration is greater than the saturation concentration of the polymer, crystallization in the solution could occur with little confinement from the water surface, leading to 2D lamellae. In fast ECWS, the evaporation rate is fast and crystallization in solution does not take place. Fast ECWS was also conducted at different temperatures (0, 60, and 80 °C in addition to the 21 °C previously discussed). Crystallization rate should gradually increase with decreasing temperature.

Figure 7 shows that at both 0 °C, similar to Figure 1, 1D filaments are formed. Detailed analysis shows that at 0 °C, uniform height of ~2 nm is achieved after 1 min of deposition, and the thickness retains when compared with the 15 min sample. For 21 °C, we observed bimodal distribution of height at 1 min, and the height becomes uniform at 15 min. This small difference may be attributed to the faster crystallization rate at 0 °C. Granular appearance of the filaments is also evident in Figure 7a,d, confirming that the 1D filaments are formed by merging of 0D clusters. At 60 °C, the 1D filaments are also seen, with a greater thickness (5 nm) and more separated. This is likely due to the slower crystallization at a higher temperature, allowing for polymer chains to laterally diffuse so that crystals can merge into larger bundles. Similar observation was seen in slow ECWS. At 80 °C, only clusters were seen, suggesting that the temperature is too high for PLLA to crystallize on water surface.

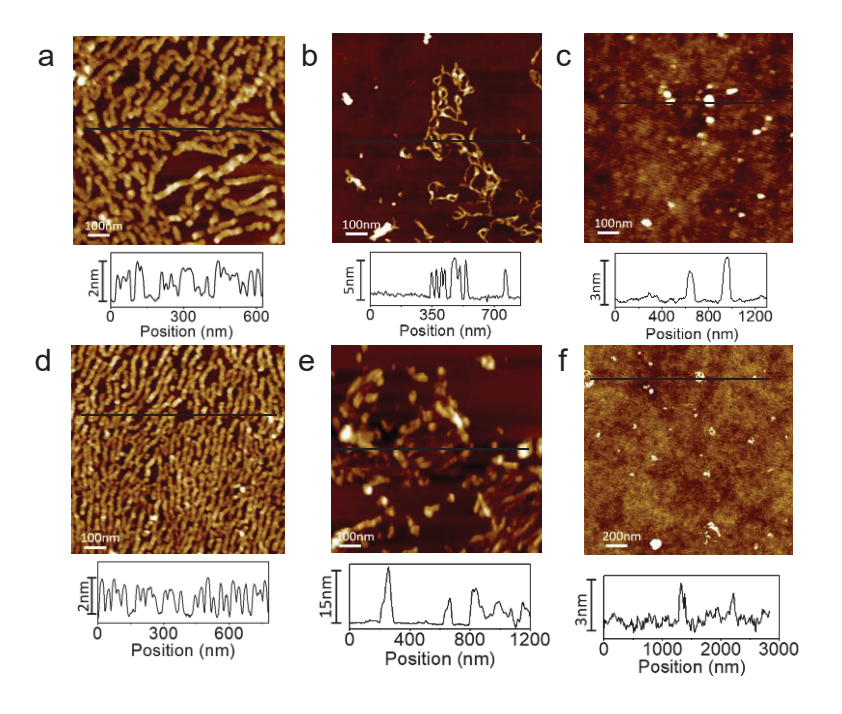


Figure 7. Temperature-dependence of PLLA crystals in ECWS. (a-f) AFM images and the corresponding height profiles of the PLLA crystals formed using 10 μ L of 0.03 wt.% PLLA solution on the water surface at 0 °C (a,d), 60°C (b,e), and 80 °C (c,f).

Conclusions

We investigated the ECWS of PLLA using fast evaporation method and compared the

results with slow evaporation in chamber and crystallization on water surface in an LB trough. Our

data show that, contrary to the 1D filament and 2D sheet biphasic morphology observed using

slow (7 h) evaporation, only 1D PLLA crystalline filaments are formed for fast evaporation (15

min). The fast evaporation results are consistent with those obtained from the crystallization of

PLLA on LB trough. For fast ECWS and crystallization in LB, rapid solvent evaporation ensures

strong confinement of water surface to the PLLA molecules. The 1D filaments are formed by

particle-mediated crystal growth. The PLLA crystalline morphology can be tuned by the polymer

concentration, crystallization temperature, and polymer molecular weight. Post annealing on water

surface shows that 1D filaments could transfer into 2D lamellae, indicating that the 2D lamellae

are the thermodynamically more stable phase.

ASSOCIATED CONTENT

Supporting Information

AFM images of ECWS of PLLA after annealing. The Supporting Information is available

free of charge on the ACS Publications website at DOI:

AUTHOR INFORMATION

Corresponding Author

* Christopher Li, E-mail: chrisli@drexel.edu

22

ORCID ID: 0000-0003-2431-7099

Author Contributions

QQ conducted the experiments and data analysis. CF analyzed the data and cowrote the manuscript. CL directed the project. The manuscript was written through the contributions of all authors.

Notes

The authors declare no competing financial interest.

ACKNOWLEDGMENT

This research was financially supported by the National Science Foundation DMR 2104968 and CMMI 1762626.

References

- (1) Michell, R. M.; Mueller, A. J. Confined crystallization of polymeric materials. *Progress in Polymer Science* **2016**, *54*, 183-213.
- (2) Staub, M. C.; Li, C. Y. Polymer crystallization at liquid-liquid interface. *Polymer Crystallization* **2018**, *I* (4), 10045.
- (3) Li, C. Y. The rise of semicrystalline polymers and why are they still interesting. *Polymer* **2020**, *211*, 123150.
- (4) Hu, W.; Frenkel, D. Effect of Metastable Liquid–Liquid Demixing on the Morphology of Nucleated Polymer Crystals. *Macromolecules* **2004**, *37* (12), 4336-4338.
- (5) Hu, W.; Frenkel, D. Polymer Crystallization Driven by Anisotropic Interactions. *Interphases and Mesophases in Polymer Crystallization III* **2005**, 1-35.
- (6) Wang, H.; Shimizu, K.; Kim, H.; Hobbie, E. K.; Wang, Z.-G.; Han, C. C. Competing growth kinetics in simultaneously crystallizing and phase-separating polymer blends. *The Journal of Chemical Physics* **2002**, *116* (16), 7311-7315.
- (7) Mitra, M. K.; Muthukumar, M. Theory of spinodal decomposition assisted crystallization in binary mixtures. *The Journal of Chemical Physics* **2010**, *132* (18), 184908.
- (8) Chuang, W.-T.; Jeng, U. S.; Hong, P.-D.; Sheu, H.-S.; Lai, Y.-H.; Shih, K.-S. Dynamic interplay between phase separation and crystallization in a poly(ε-caprolactone)/poly(ethylene glycol) oligomer blend. *Polymer* **2007**, *48* (10), 2919-2927.

- (9) Schaaf, P.; Lotz, B.; Wittmann, J. C. Liquid-liquid phase separation and crystallization in binary polymer systems. *Polymer* **1987**, *28* (2), 193-200.
- (10) Zhou, J.; Man, X.; Jiang, Y.; Doi, M. Structure Formation in Soft-Matter Solutions Induced by Solvent Evaporation. *Advanced Materials* **2017**, *29* (45), 1703769.
- (11) Routh, A. F. Drying of thin colloidal films. Reports on Progress in Physics 2013, 76 (4), 046603.
- (12) Tang, Q.; Müller, M.; Li, C. Y.; Hu, W. Anomalous Ostwald Ripening Enables 2D Polymer Crystals via Fast Evaporation. *Physical Review Letters* **2019**, *123* (20), 207801.
- (13) Cummings, J.; Lowengrub, J. S.; Sumpter, B. G.; Wise, S. M.; Kumar, R. Modeling solvent evaporation during thin film formation in phase separating polymer mixtures. *Soft Matter* **2018**, *14* (10), 1833-1846, 10.1039/C7SM02560B.
- (14) Yuan, Y.; Zhang, J.; Sun, J. Effect of Solvent Evaporation Rate on Order-to-Disorder Phase Transition Behavior of Regioregular Poly(3-butylthiophene). *Macromolecules* **2011**, *44* (15), 6128-6135.
- (15) Higuchi, T.; Motoyoshi, K.; Sugimori, H.; Jinnai, H.; Yabu, H.; Shimomura, M. Phase Transition and Phase Transformation in Block Copolymer Nanoparticles. *Macromolecular Rapid Communications* **2010**, *31* (20), 1773-1778.
- (16) Kovalchuk, N. M.; Trybala, A.; Starov, V. M. Evaporation of sessile droplets. *Current Opinion in Colloid & Interface Science* **2014**, *19* (4), 336-342.
- (17) Okulova, N.; Johansen, P.; Christensen, L.; Taboryski, R. Effect of Structure Hierarchy for Superhydrophobic Polymer Surfaces Studied by Droplet Evaporation. *Nanomaterials* **2018**, *8* (10), 831.
- (18) Parsa, M.; Harmand, S.; Sefiane, K. Mechanisms of pattern formation from dried sessile drops. *Advances in Colloid and Interface Science* **2018**, *254*, 22-47.
- (19) Park, M. S.; Aiyar, A.; Park, J. O.; Reichmanis, E.; Srinivasarao, M. Solvent Evaporation Induced Liquid Crystalline Phase in Poly(3-hexylthiophene). *Journal of the American Chemical Society* **2011**, *133* (19), 7244-7247.
- (20) Song, T.; Wu, X.; Xu, J.; Ye, H.; Shi, W. Two-Level Optical Birefringence Created by Evaporation-Induced Polymer Crystallization in Sessile Droplets. *Macromolecules* **2023**, *56* (2), 707-718.
- (21) Li, Y.; Huang, H.; Wang, Z.; He, T. Tuning radial lamellar packing and orientation into diverse ring-banded spherulites: Effects of structural feature and crystallization condition. *Macromolecules* **2014**, *47* (5), 1783-1792.
- (22) Li, Y.; Wang, Z.; He, T. Morphological control of polymer spherulites via manipulating radial lamellar organization upon evaporative crystallization: A mini review. *Crystals* **2017**, *7* (4), 115.
- (23) Alamo, R. G.; Jeon, K.; Smith, R.; Boz, E.; Wagener, K. B.; Bockstaller, M. Crystallization of polyethylenes containing chlorines: Precise vs random placement. *Macromolecules* **2008**, *41* (19), 7141-7151.
- (24) Wang, W.; Qi, H.; Zhou, T.; Mei, S.; Han, L.; Higuchi, T.; Jinnai, H.; Li, C. Y. Highly robust crystalsome via directed polymer crystallization at curved liquid/liquid interface. *Nature communications* **2016**, *7*, 10599.
- (25) Wang, W.; Staub, M. C.; Zhou, T.; Smith, D. M.; Qi, H.; Laird, E. D.; Cheng, S.; Li, C. Y. Polyethylene nano crystalsomes formed at a curved liquid/liquid interface. *Nanoscale* **2018**, *10* (1), 268-276.

- (26) Qi, H.; Zhou, H.; Tang, Q.; Lee, J. Y.; Fan, Z.; Kim, S.; Staub, M. C.; Zhou, T.; Mei, S.; Han, L. Block copolymer crystalsomes with an ultrathin shell to extend blood circulation time. *Nature communications* **2018**, *9* (1), 3005.
- (27) Staub, M. C.; Li, R.; Fukuto, M.; Li, C. Y. Confined Crystal Melting in Edgeless Poly (1-lactic acid) Crystalsomes. *ACS Macro Letters* **2020**, *9* (12), 1773-1778.
- (28) Qi, H.; Liu, X.; Henn, D. M.; Mei, S.; Staub, M. C.; Zhao, B.; Li, C. Y. Breaking translational symmetry via polymer chain overcrowding in molecular bottlebrush crystallization. *Nature Communications* **2020**, *11* (1), 2152.
- (29) Staub, M. C.; Kim, S.; Yu, S.; Li, C. Y. Porous Crystalsomes via Emulsion Crystallization and Polymer Phase Separation. *ACS Macro Letters* **2022**, *11*, 1022-1027.
- (30) Staub, M. C.; Yu, S.; Li, C. Y. Poly (3-hexylthiophene)(P3HT) Crystalsomes: Tiling 1D Polymer Crystals on a Spherical Surface. *Macromolecular Rapid Communications* **2022**, 2200529.
- (31) Staub, M. C.; Yu, S.; Li, C. Y. Colloidosome-Templated Poly (L-lactic acid) Crystalsomes. *Giant* **2022**, 100124.
- (32) Gao, L.; Mei, S.; Qian, Q.; Yu, S.; Zhao, B.; Tu, Y.; Li, C. Y. Crystallization-driven Nanoparticle Crystalsomes. *Angewandte Chemie International Edition* **2023**, *62* (15), e202217267.
- (33) Li, B.; Esker, A. R. Molar mass dependent growth of poly(epsilon-caprolactone) crystals in Langmuir films. *Langmuir* **2007**, *23* (5), 2546-2554.
- (34) Li, B.; Esker, A. R. Blends of poly(epsilon-caprolactone) and intermediate molar mass polystyrene as langmuir films at the air/water interface. *Langmuir* **2007**, *23* (2), 574-581.
- (35) Li, B.; Wu, Y.; Liu, M.; Esker, A. R. Brewster angle microscopy study of poly(epsilon-caprolactone) crystal growth in Langmuir films at the air/water interface. *Langmuir* **2006**, *22* (11), 4902-4905.
- (36) Fuchs, C.; Busse, K.; Flieger, A. K.; Kressler, J. Polymer crystallization on the surface of water or aqueous salt solution. *Chemical Engineering & Technology* **2016**, *39* (7), 1333-1340.
- (37) Hasan, N.; Fuchs, C.; Schwieger, C.; Busse, K.; Dolynchuk, O.; Kressler, J. Crystallization of poly (ε-caprolactone) at the air-water interface studied by IRRAS and GI-WAXS. *Polymer* **2020**, *196*, 122468.
- (38) Ni, S.; Yin, W.; Ferguson-McPherson, M. K.; Satija, S. K.; Morris, J. R.; Esker, A. R. Nanoscale surface patterns from 103 single molecule helices of biodegradable poly (L-lactic acid). *Langmuir* **2006**, *22* (14), 5969-5973.
- (39) Ni, S.; Lee, W.; Li, B.; Esker, A. R. Thermodynamics of the liquid expanded to condensed phase transition of poly (L-lactic acid) in Langmuir monolayers. *Langmuir* **2006**, *22* (8), 3672-3677.
- (40) Iwashima, K.; Yamamoto, T.; Tezuka, Y.; Kumaki, J. Self-Assembly of linear and cyclic polylactide stereoblock copolymers with a parallel and antiparallel chain arrangement distinguishing their directions on a water surface. *Langmuir* **2020**, *36* (22), 6216-6221.
- (41) Watanabe, K.; Kumaki, J. Extended-chain crystallization and stereocomplex formation of polylactides in a Langmuir monolayer. *Polymer Journal* **2020**, *52* (6), 601-613.
- (42) Das, A.; El-Tawargy, A. S.; Khechine, E.; Noack, S.; Schlaad, H.; Reiter, G. n.; Reiter, R. Controlling nucleation in quasi-two-dimensional Langmuir poly (l-lactide) films through variation of the rate of compression. *Langmuir* **2019**, *35* (18), 6129-6136.
- (43) Das, A.; Noack, S.; Schlaad, H.; Reiter, G. n.; Reiter, R. Exploring pathways to equilibrate Langmuir polymer films. *Langmuir* **2020**, *36* (28), 8184-8192.

- (44) Xu, X.; Shao, Y.; Wang, W.; Liu, H.; Zhang, W.; Yang, S. Morphological variation of an LB film of giant amphiphiles composed of poly (ethylene oxide) and hydrophobically modified POSS. *Langmuir* **2021**, *37* (14), 4294-4301.
- (45) Wang, W.-J.; Xu, X.; Shao, Y.; Liao, J.-W.; Jian, H.-X.; Xue, B.; Yang, S.-G. Fractal growth of giant amphiphiles in langmuir-blodgett films. *Chinese Journal of Polymer Science* **2022**, *40* (6), 556-566.
- (46) Qi, H.; Wang, W.; Li, C. Y. Janus Polymer Single Crystal via Evaporative Crystallization. *ACS Macro. Lett.* **2014**, *3*, 675-678.
- (47) Qian, Q.; Yu, S.; Li, C. Y. Tuning Poly (l-lactic acid) Crystallization Pathways via Evaporative Crystallization on a Water Surface. *Macromolecules* **2023** *56*, 8747–8753.
- (48) Strobl, G. From the melt via mesomorphic and granular crystalline layers to lamellar crystallites: A major route followed in polymer crystallization? *The European Physical Journal E* **2000**, *3* (2), 165-183, journal article.
- (49) Strobl, G. Crystallization and melting of bulk polymers: New observations, conclusions and a thermodynamic scheme. *Progress in Polymer Science* **2006**, *31* (4), 398-442.
- (50) De Yoreo, J. J.; Gilbert, P. U.; Sommerdijk, N. A.; Penn, R. L.; Whitelam, S.; Joester, D.; Zhang, H.; Rimer, J. D.; Navrotsky, A.; Banfield, J. F. Crystallization by particle attachment in synthetic, biogenic, and geologic environments. *Science* **2015**, *349* (6247).
- (51) Chen, X.; Wang, W.; Cheng, S.; Dong, B.; Li, C. Y. Mimicking Bone Nanostructure by Combining Block Copolymer Self-Assembly and 1D Crystal Nucleation. *ACS Nano* **2013**, 7, 8251-8257.
- (52) Gleeson, S. E.; Kim, S.; Yu, T.; Marcolongo, M.; Li, C. Y. Insight on the Role of Poly (acrylic acid) for Directing Calcium Phosphate Mineralization of Synthetic Polymer Bone Scaffolds. *ACS Applied Bio Materials* **2022**, *5* (9), 4493-4503.
- (53) Wasanasuk, K.; Tashiro, K.; Hanesaka, M.; Ohhara, T.; Kurihara, K.; Kuroki, R.; Tamada, T.; Ozeki, T.; Kanamoto, T. Crystal structure analysis of poly (l-lactic acid) α form on the basis of the 2-dimensional wide-angle synchrotron X-ray and neutron diffraction measurements. *Macromolecules* **2011**, *44* (16), 6441-6452.

Table of Contents

